Mechanical Systems and Signal Processing 135 (2020) 106326

Contents lists available at ScienceDirect

Mechanical Systems and Signal Processing

journal homepage: www.elsevier.com/locate/ymssp

Efficient swing control of an overhead crane with simultaneous payload hoisting and external disturbances

Liyana Ramli [a], Z. Mohamed [a,*], M.Ö. Efe [b], Izzuddin M. Lazim [a], H.I. Jaafar [a,c]

[a] School of Electrical Engineering, Universiti Teknologi Malaysia, Johor, Malaysia
[b] Department of Computer Engineering, Hacettepe University, Turkey
[c] Faculty of Electrical Engineering, Universiti Teknikal Malaysia Melaka, Melaka, Malaysia

ARTICLE INFO

Article history:
Received 17 May 2019
Received in revised form 22 July 2019
Accepted 21 August 2019
Available online 11 September 2019

Keywords:
Disturbance
Hoisting
Input shaping
Neural network
Overhead crane
PID
Swing control

ABSTRACT

The effects of time varying parameters and external disturbances on a flexible system may badly degrade the control performance resulting in excessive induced vibrations/oscillations. For an overhead crane, the oscillation can be even worse when both factors occur simultaneously. This paper proposes a novel swing control approach for an underactuated overhead crane having payload hoisting and external disturbance simultaneously. The proposed scheme is designed based on a predictive unity magnitude shaper and an adaptive feedback control which efficiently suppress payload swing to handle both effects. Furthermore, the control parameters can be updated online in real time to progressively suppress the payload swing. To evaluate the effectiveness of the proposed method, experiments are carried out with a simultaneous payload hoisting and external disturbances including a non-zero initial condition, persistent disturbance (wind) and instant disturbance. The developed controller achieves higher robustness under all testing conditions with significant swing reductions of at least 45% and 69% in the overall and residual swing responses, respectively over a comparative control method. It is envisaged that the proposed method can be very beneficial as an anti-swing controller for various cranes under the influence of disturbance and hoisting simultaneously.

1. Introduction

Cranes offer transportation services of heavy loads that are widely utilized in many sectors around the globe such as in constructions, factories and marine industries. However, owing to its flexible structure, it may suffer from excessive swing due to incompetence of human operator to handle the crane and the existence of unexpected external disturbances. In addition, payload hoisting which is an essential crane operation might also lead to higher payload swing, bouncing and twisting. Hence, it is crucial to design efficient controllers that can eliminate the excessive swing subjected to these factors to achieve a fast operation, a safe workplace, and to avoid damage to the load quality and neighbouring facilities. Various vibration control algorithms for crane systems have been widely designed for a single pendulum crane system [1–3], a double pendulum crane system [4,5] and a dual crane system [6]. In addition, numerous types of controllers comprising feedforward and feedback control for crane systems have been reviewed in [7].

* Corresponding author.
E-mail address: zahar@fke.utm.my (Z. Mohamed).

https://doi.org/10.1016/j.ymssp.2019.106326
0888-3270/

Input shaping is a feedforward control technique that has been utilized pervasively to reduce the induced oscillations/vibrations of the flexible systems [4,8–10]. A shaper that can effectively eliminate the oscillations whilst producing a fast response with a shorter shaper duration is desirable for a crane control system. One of the shapers that can meet these criteria is known as a unity magnitude zero vibration (UMZV) which resembles a finite actuated oscillatory system [11]. In crane operations, varying cable length during payload hoisting and using different payload masses cause system's natural frequency and damping ratio to change. Since the shaper's design is highly dependent on these parameters, the performance of the shaper based on fixed system parameters becomes weak and incompetent to handle the effects. To tackle this issue, recently a predictive UMZV shaper using a neural network (NNUMZV) approach was proposed [12]. Using the NNUMZV, the parameters of the shaper can be updated in real-time considering the change in payload mass and cable length to yield an accurate shaper design. However, when the payload experiencing a large swing due to the existence of external disturbances, operating crane becomes more challenging. These include the effects of non-zero initial condition [13], wind disturbance [14,15] and several other external disturbances [16,17] that have been considered for crane systems. Consequently, the performance of NNUMZV tends to deteriorate implying its incapability in handling these disturbances. Recently, a robust control has been implemented as it can handle the effect of disturbances effectively for crane [18], vehicle systems [19,20] and DC motor [21].

Several works have been reported for payload swing control of cranes with payload hoisting and disturbance. These include feedforward, feedback and a combined feedforward and feedback controllers. Within the combined controller, a proportional integral derivative plus proportional derivative control (PIDPD) [22] and an optimal PID controller [23] were proposed as an anti-swing control for a gantry crane system. However, these control schemes only considered a case with changing cable length. A combined control utilizing a feedback and feedforward schemes was also designed as an anti-swing control to eliminate the excessive oscillations resulted from the external disturbance [14,15]. However, the feedback control was not designed to aggressively eliminate the oscillation to avoid from unexpected motions that would surprise the human operator [14]. Numerous control schemes were designed to tackle the effects of payload hoisting in various cranes [24–32]. Similarly, control schemes to cater both the external disturbances and payload hoisting effects were also developed [16,33–38]. However, it was found that most of the work considered them separately. It is worthwhile to point out that the crane control challenge increases under both effects simultaneously.

Motivated to overcome the issue, this paper proposes a novel control scheme for efficient swing control of an overhead crane with simultaneous payload hoisting and external disturbances. The main difference between the current paper and the previously developed predictive NNUMZV [12] involves hybridization of the predictive NNUMZV and an adaptive PID like neural network (APIDLNN) controller. The control scheme is implemented on an overhead crane experimental testbed and tested under three experimental cases involving payload hoisting, a non-zero initial condition, persistent disturbance (wind) and instant disturbance. A PID-based PSO (PIDPSO) controller is also designed as a comparative method to verify the effectiveness of the proposed controller in terms of the overall payload swing and residual swing. The merits of the paper can be summarized as:

1. The proposed hybrid control scheme involves the NNUMZV shaper that can predict and update the shaper parameters in real-time to handle payload hoisting, and the APIDLNN which are adapted online based on the gradient descent method to cater the effect of external disturbances. Furthermore, to achieve a faster convergence, the weights initialization of APIDLNN is optimized using the particle swarm optimization (PSO).
2. This paper contributes in the control structure that combines the predictive input shaping and the APIDLNN control for swing suppression under the effect of simultaneous payload hoisting and external disturbance. Within crane control, only limited work has been reported in control of both effects simultaneously, especially in the real-time implementation involving several types of disturbances. A series of hardware experiments are carried out to verify the effectiveness and robustness of the proposed swing control.
3. Most of the existing control methods for the overhead crane were designed under a small swing assumption which requires linearization of the nonlinear model. However, in real application, the effects of payload hoisting and existence of external disturbances such as wind or collision could induce a large swing which increase the difficulty to guarantee the control performance. In this paper, the proposed hybrid controller is designed based on a nonlinear model with learning capability and strong robustness features to handle the effects. A sufficient closed-loop stability analysis is proven, implying the effectiveness of the learning algorithm and varied learning rates.

The rest of the paper is organized as follows. Section 2 describes the mathematical model of a 2-degree-of-freedom overhead crane with hoisting, and hardware descriptions of the overhead crane testbed. Section 3 presents the previously developed controller that needs to be enhanced whereas Section 4 explains the structure of the proposed NNUMZV-APIDLNN, together with the details of adaptation algorithm. Section 5 demonstrates the experimental results to show the superiority of the proposed controller, and finally concluding remarks are given in Section 6.

2. Model description

Fig. 1 illustrates a plane model of a two-dimensional (2-D) overhead crane. A distance r indicates a path taken by the trolley from the origin, up to the suspension point of the cable on the trolley. l, m and θ represent the hoisting cable length,

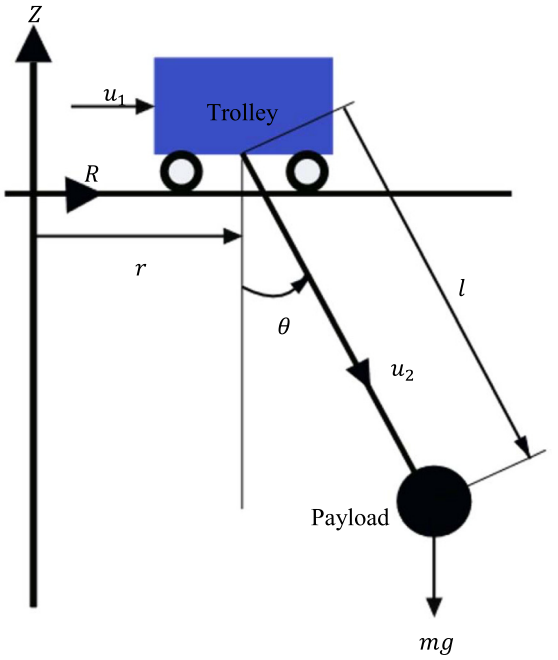

Fig. 1. A plane model of a two-dimensional overhead crane with hoisting payload.

payload mass and swing angle, respectively. u_1 and u_2 denote the driving forces for r and l motions, respectively. The equations of motion of the crane system are given as [39]

$$(m_r + m)\ddot{r} + ml\cos\theta\ddot{\theta} + m\sin\theta\ddot{l} + b_x\dot{r} + 2m\cos\theta\dot{l}\dot{\theta} - ml\sin\theta\dot{\theta}^2 = u_1 \tag{1}$$

$$m\ddot{l} + m\sin\theta\ddot{r} + b_l\dot{l} - ml\dot{\theta}^2 - mg\cos\theta = u_2 \tag{2}$$

$$ml^2\ddot{\theta} + ml\cos\theta\ddot{r} + 2ml\dot{l}\dot{\theta} + mgl\sin\theta = 0 \tag{3}$$

where m_r is the travelling components of crane mass that includes the equivalent masses of the rotating parts, g is the gravitational acceleration, and b_x and b_l represent the viscous damping coefficients for the r and l motions, respectively. The mass and stiffness of the cable and the viscous damping in the payload swing are neglected and the payload is assumed as a point mass.

3. Unity-magnitude zero vibration (UMZV) input shaping

Input shaping is an effective feedforward control for suppressing vibrations of a flexible system. By using input shaping, the system's vibration is reduced by convolving the command input signal with a sequence of impulses of which produces zeros over each of the flexible pole [40]. Apart from utilizing zero vibration-type shapers that contain positive impulse amplitudes, a shorter shaper could be obtained if negative impulse amplitudes are considered [11,41]. The impulse amplitudes are constrained to be 1 or -1 to achieve a time-optimal command. One of the negative input shapers is the UMZV and is given as [11,41]

$$\begin{bmatrix} A_i \\ t_i \end{bmatrix} = \begin{bmatrix} 1 & -1 & 1 \\ 0 & t_2 & t_3 \end{bmatrix} \tag{4}$$

where A_i and t_i are the amplitude and time location of the impulse respectively. t_i can be defined as

$$\begin{bmatrix} t_2 \\ t_3 \end{bmatrix} = \begin{bmatrix} \frac{2\pi}{\omega_d\left(1/6+0.272\zeta+0.203\zeta^2\right)} \\ \frac{2\pi}{\omega_d\left(1/3+0.005\zeta+0.179\zeta^2\right)} \end{bmatrix} \tag{5}$$

where $\omega_d = \omega_n(\sqrt{1-\zeta^2})$. ω_n and ζ represent natural frequency and damping ratio of the system respectively.

As a conventional shaper is designed based on a linear plant, the shaper's performance tends to deteriorate for a nonlinear system. Recently, to handle nonlinearities and changes in the natural frequencies and damping ratio, a neural network based

UMZV (NNUMZV) shaper was proposed. In this approach, optimal shaper parameters were obtained using the NN subjected to varying cable lengths due to the payload hoisting and changes in payload mass as shown in Fig. 2. The NN structure used in Fig. 2 represents a simple structure of feedforward neural network with three layers since this structure is adequate to predict the shaper's parameters accurately with less computational complexity. Nevertheless, other types of NN can also be implemented to predict the shaper's parameters.

A detailed description on the application of NN for designing a real time UMZV shaper can be found in [7]. However, the control scheme was unable to handle payload swing due to the external disturbances which are common in industrial operation scenarios. This paper aims to enhance the work [7] to cater simultaneous payload hoisting and external disturbances, by proposing a control structure as discussed in the following section.

4. NNUMZV-APIDLNN algorithm

In this work, an efficient swing control is designed based on the NNUMZV shaper and APIDLNN under simultaneous payload hoisting and several types of external disturbances. APIDLNN offers both the simplicity of PID control and the self-learning ability of NN [42]. Fig. 3 shows the proposed control structure where $R, \theta, \theta_d, u_c, u_s, u_1$ and e represent the input signal, actual swing angle, desired swing angle, APIDLNN control signal, NNUMZV shaped signal, control input and swing error respectively. The control structure can be viewed as a combination of feedforward and feedback controllers as shown with the dotted lines in Fig. 3.

Based on a measured cable length, the NNUMZV shaper determines optimal shaper parameters to tackle payload swing due to the payload hoisting. This results in a shaped input, u_1 which is applied to the system. At the same time, the actual payload swing which is also affected by the external disturbances is processed using the APIDLNN and fed back to the system. In this work, a positive feedback is utilized, as the approach was successfully implemented in [22,23] for control of cranes.

Fig. 4 illustrates the network structure of the APIDLNN adopted in this work that consists of 3 layers known as input (i), hidden (j) and output (k) layers. The parameters of h_{ij} and o_{jk} represent the weights between input and hidden layers and the weights between hidden and output layers respectively. The input layer contains one input node that will receive the error signal, e and directly send it to the weighted sum nodes $X_j(j = 1, .., n_j)$ in the hidden layer. The other nodes in hidden layer represent the proportional node Q_1, the integral node Q_2 and the differential node Q_3, and z^{-1} is a unit delay operator. An output node in the output layer will directly send the feedback control signal, u_2 into the system.

The outputs of hidden layer represented by Q_1, Q_2 and Q_3 neurons are,

$$Q_1(N) = g(X_1(N)) = g(h_{11}(N)e(N)) \tag{6}$$

$$Q_2(N) = g(X_2(N)) = g(h_{12}(N)e(N) + \ Q_2(N-1)) \tag{7}$$

$$Q_3(N) = g(X_3(N)) = g(h_{13}(N)e(N) - \ h_{13}(N-1)e(N-1)) \tag{8}$$

where N is the number of iteration and the error, $e(N) = \theta_d(N) - \theta(N)$. The function $g(x)$ is given as,

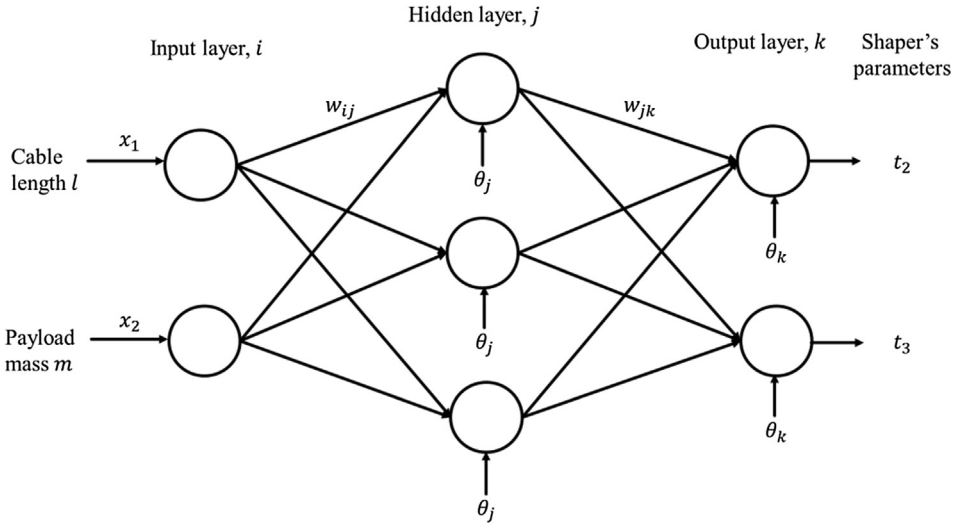

Fig. 2. Network structure of the NNUMZV shaper.

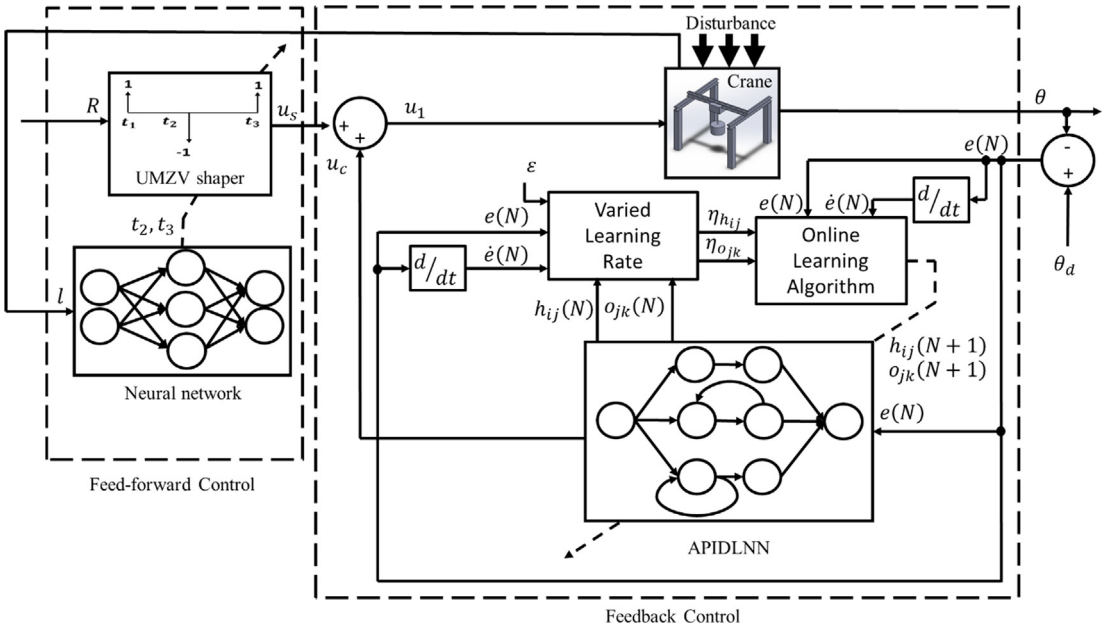

Fig. 3. A combined control structure.

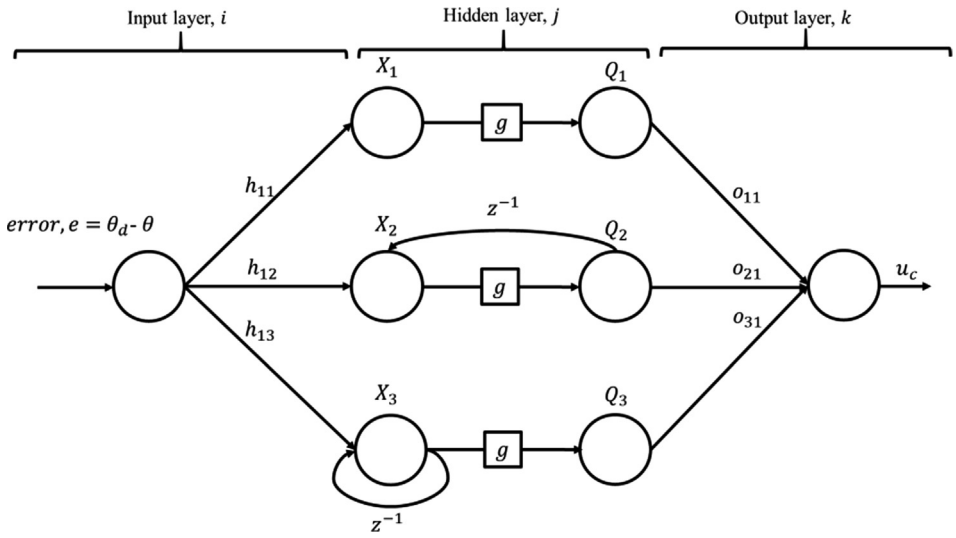

Fig. 4. Network structure of the APIDLNN.

$$g(x) = \begin{cases} 1 & x \geqslant 1 \\ x & -1 < x < 1 \\ -1 & x \leqslant -1 \end{cases} \tag{9}$$

The upper and lower bounds of function $g(x)$ ensure that the signal does not grow uncontrollably as it propagates from one layer to the next. The final output of the APIDLNN can be expressed as,

$$c(N) = \sum_{j=1}^{n_j} o_{j1}(N) Q_j(N) \tag{10}$$

where $n_j = 3$ is the number of neurons in the hidden layer. Based on Equations (6)-(10), $Q_2(N)$ can be written as

$$Q_2(N) = \frac{h_{12}(N) e(N)}{1 - z^{-1}} \tag{11}$$

where Eq. (11) has the relationship of integral and $Q_2(N)$ is known as an integral node. On the other hand, $Q_3(N)$ can be written as

$$Q_3(N) = (h_{13}(N)e(N))(1 - z^{-1}) \tag{12}$$

in which Eq. (12) has the relationship of differential and $Q_3(N)$ is known as a differential node.

4.1. Weight initialization

This section describes the optimization of APIDLNN initial weights (h_{ij} and o_{jk}) using PSO, prior to the real-time implementation. Instead of assuming them randomly, these optimal initial weights were obtained offline to ensure a faster convergence of the actual weights during real-time adaptation of the APIDLNN. By assuming them randomly or by using different initial values would affect the effectiveness of training process of the APIDLNN during online adaptation, resulting in unsatisfactory swing reduction. By optimizing these values, the training session during real-time adaptation can be reduced since the starting point of the optimization is very close to the global minimum.

The control variables of the PSO were set as weights of the network which correspond to the position vector of the i^{th} particle in the search space. The range for each control variable was tuned between $[-1,1]$ with a population size of 40. Each particle can be assigned as a point in a D-dimensional space and the position of i^{th} particle, x_i will be updated according to the given velocity update to finally reach an optimal solution in the search space area. Two best values were evaluated in the population called personal best, pb and global best, gb. The velocity of the i^{th} particle is given by

$$v_{id}^{t+1} = \omega v_{id}^{t} + \gamma_1 r_{1d}^{t}\left[pb_{id}^{t} - x_{id}^{t}\right] + \gamma_2 r_{2d}^{t}\left[gb_{d}^{t} - x_{id}^{t}\right] \tag{13}$$

$$x_{id}^{t+1} = x_{id}^{t} + v_{id}^{t+1} \tag{14}$$

where $d \in [1, D]$ and $i \in [1, s]$. s and t are the number of particle and current iteration number respectively. The acceleration coefficients, γ_1 and γ_2 were set as 1.5 and the random numbers, r_1 and r_2 were assigned between $[0, 1]$. Inertia weight, ω that controls the momentum and the capability in terms of exploration and exploitation of the particles toward finding a good optimal point is given as

$$\omega^{t+1} = \omega_{max} - \left(\frac{\omega_{max} - \omega_{min}}{t_{max}}\right)t \tag{15}$$

where ω_{max} and ω_{min} are the maximum and minimum values of inertia weight that were set as 0.9 and 0.4, respectively. t_{max} is the maximum iteration number. All particles were evaluated based on the fitness function, J aimed to reduce the payload swing angle which is based on mean square error (MSE), given as

$$J = \int_0^T |\theta_d - \theta|^2 dt \tag{16}$$

where T is the time of simulation. The fitness value of each particle was calculated in every iteration to finally find the optimal initial weights. The optimization process was carried out by using simulation in Matlab and the results are as shown in Table 1.

4.2. Online learning algorithm

The online learning algorithm in Fig. 3 utilized the gradient descent method to adjust weights of the network. The cost function E is defined as,

$$E(N) = \frac{1}{2}[\theta_d(N) - \theta(N)]^2 = \frac{1}{2}e^2(N) \tag{17}$$

The updating weights are obtained by means of minimizing the cost function, E. In the output layer, the error term to be propagated is computed as,

$$\delta_o(N) = -\frac{\partial E(N)}{\partial u_c(N)} = -\frac{\partial E(N)}{\partial e(N)}\frac{\partial e(N)}{\partial u_c(N)} = -\frac{\partial E(N)}{\partial e(N)}\frac{\partial e(N)}{\partial \theta(N)}\frac{\partial \theta(N)}{\partial u_c(N)} \tag{18}$$

Table 1
Optimized initial gains of APIDLNN.

Initial weight	h_{11}	h_{12}	h_{13}	o_{11}	o_{21}	o_{31}
Value	1	−0.0049	−0.2832	−1	−0.1670	−0.2562

The term $\frac{\partial\theta(N)}{\partial u_c(N)}$ cannot be easily obtained due to uncertain dynamics of the system. Hence, to solve this problem whilst speeding up the online learning process, δ_o can be approximated as [43],

$$\delta_o \cong (\theta_d(N) - \theta(N)) + \left(\dot{\theta}_d(N) - \dot{\theta}(N)\right) = e + \dot{e} \tag{19}$$

and the weight o_{jk} can be updated by,

$$o_{jk}(N+1) = o_{jk}(N) + \Delta o_{jk}(N) \tag{20}$$

where $\Delta o_{jk}(N) = -\eta_{o_{jk}} \frac{\partial E(N)}{\partial o_{jk}(N)}$ and $\eta_{o_{jk}}$ is the learning rate between the hidden layer and the output layer. By applying the chain rule of the network layers,

$$\frac{\partial E(N)}{\partial o_{jk}(N)} = \frac{\partial E(N)}{\partial u_c(N)} \frac{\partial u_c(N)}{\partial o_{jk}(N)} \tag{21}$$

Eq. (21) can be written as,

$$\frac{\partial E(N)}{\partial o_{jk}(N)} = -\delta_o(N) Q_j(N) \tag{22}$$

On the other hand, the weight h_{ij} can be updated by,

$$h_{ij}(N+1) = h_{ij}(N) + \Delta h_{ij}(N) \tag{23}$$

where $\Delta h_{ij}(N) = -\eta_{h_{ij}} \frac{\partial E(N)}{\partial h_{ij}(N)}$ and $\eta_{h_{ij}}$ is the learning rate between the input layer and the hidden layer. The partial derivative of $E(N)$ with respect to $h_{ij}(N)$ is formulated as,

$$\frac{\partial E(N)}{\partial h_{ij}(N)} = \frac{\partial E(N)}{\partial u_c(N)} \frac{\partial u_c(N)}{\partial Q_j(N)} \frac{\partial Q_j(N)}{\partial X_j(N)} \frac{\partial X_j(N)}{\partial h_{ij}(N)} \tag{24}$$

The derivative, $\frac{\partial Q_j(N)}{\partial X_j(N)}$ can be approximated by its sign function, $\mathrm{sgn}\left(\frac{Q_j(N) - Q_j(N-1)}{X_j(N) - X_j(N-1)}\right)$ as described in [44]. Eq. (24) can then be rewritten as,

$$\frac{\partial E(N)}{\partial h_{ij}(N)} = -\delta_o(N) o_{jk}(N) \mathrm{sgn}\left(\frac{Q_j(N) - Q_j(N-1)}{X_j(N) - X_j(N-1)}\right) e(N) \tag{25}$$

The online learning algorithm will keep updating the next iteration weight values ($o_{jk}(N+1)$ and $h_{ij}(N+1)$) in Eqs. (20) and (23), based on the calculated values of $\Delta h_{ij}(N)$ and $\Delta o_{jk}(N)$. These equations are important in adjusting the weights online caused by the effects of the external disturbances. The learning rates ($\eta_{o_{jk}}$ and $\eta_{h_{ij}}$) are calculated in the varied learning rate block as shown in Fig. 3.

4.3. Convergence analysis

A proper design of learning rate is crucial as it determines the network performances. Hence, varied learning rates with a guaranteed convergence of tracking error is desirable which can lead to an effective training process of the APIDLNN. One can have a larger learning rate for a point far away from a global minimum and a smaller learning rate for a point closer to the global minimum. To achieve this, a discrete-type Lyapunov function [45] was adopted to design the learning rate parameters of the APIDLNN, given as

$$E(N) = \frac{1}{2} e^2(N) \tag{26}$$

The change in the Lyapunov function can be obtained as

$$\Delta E(N) = E(N+1) - E(N) \tag{27}$$

The Lyapunov function for the next iteration can be approximated as [45]

$$E(N+1) \approx E(N) + \sum_{j=1}^{3} \left[\frac{\partial E(N)}{\partial o_{j1}(N)} \Delta o_{j1}\right] + \sum_{j=1}^{3} \left[\frac{\partial E(N)}{\partial h_{1j}(N)} \Delta h_{1j}\right] \tag{28}$$

$$= \frac{1}{2} E(N) - \sum_{j=1}^{3} \eta_{o_{j1}} \left[\frac{\partial E(N)}{\partial u_c(N)} \frac{\partial u_c(N)}{\partial o_{j1}(N)}\right]^2 + \frac{1}{2} E(N) - \sum_{j=1}^{3} \eta_{h_{1j}} \left[\frac{\partial E(N)}{\partial u_c(N)} \frac{\partial u_c(N)}{\partial Q_j(N)} \frac{\partial Q_j(N)}{\partial X_j(N)} \frac{\partial X_j(N)}{\partial h_{1j}(N)}\right]^2$$

where Δo_{j1} represents the weight change between the hidden and output layers, while Δh_{1j} indicates the weight change between the input and hidden layers. The learning rate parameters can be designed as [43,45]

$$\eta_{h_{ij}} = \frac{E(N)}{2\left[\sum_{j=1}^{3}\left(\frac{\partial E(N)}{\partial u_c(N)}\frac{\partial u_c(N)}{\partial Q_j(N)}\frac{\partial Q_j(N)}{\partial X_j(N)}\frac{\partial X_j(N)}{\partial h_{1j}(N)}\right)^2 + \varepsilon\right]} \tag{29}$$

$$\eta_{o_{jk}} = \frac{E(N)}{2\left[\sum_{j=1}^{3}\left(\frac{\partial E(N)}{\partial u_c(N)}\frac{\partial u_c(N)}{\partial o_{j1}(N)}\right)^2 + \varepsilon\right]} \tag{30}$$

where ε is a positive constant. Therefore, Eq. (28) can be approximated as [45]

$$E(N+1) \approx \varepsilon\left(\eta_{h_{ij}} + \eta_{o_{jk}}\right) = \frac{E(N)\varepsilon}{2\left[\sum_{j=1}^{3}\left(\frac{\partial E(N)}{\partial u_c(N)}\frac{\partial u_c(N)}{\partial Q_j(N)}\frac{\partial Q_j(N)}{\partial X_j(N)}\frac{\partial X_j(N)}{\partial h_{1j}(N)}\right)^2 + \varepsilon\right]} + \frac{E(N)\varepsilon}{2\left[\sum_{j=1}^{3}\left(\frac{\partial E(N)}{\partial u_c}\frac{\partial u_c(N)}{\partial o_{j1}(N)}\right)^2 + \varepsilon\right]} < \frac{E(N)}{2} + \frac{E(N)}{2}$$

$$= E(N) \tag{31}$$

For the feedback loop, Eq. (31) shows that the output error between the desired and actual payload swing responses, e will converge to zero gradually and the stability of the feedback controller can be assured. As the feedforward and closed-loop controllers were designed independently, the feedforward control does not affect the stability of the closed loop system. Furthermore, input shaping was designed outside the feedback loop as shown in Fig. 3 and thus, it has no effect on the eigenvalues of the closed-loop system as it simply modifies the command signal to the system. Hence, the stability of the overall system can be guaranteed. The implementation of input shaping within the feedback loop which can affect the closed-loop stability was discussed in [46].

The varied learning rate parameters in Eqs. (29) and (30) can guarantee the convergence of the output error based on the analysis of the discrete Lyapunov function to yield an effective training for the APIDLNN. The experimental results presented in the section revealed the effectiveness of the online learning APIDLNN model based on the adaptation algorithm and varied learning rate parameters.

5. Implementation and results

Fig. 5a shows an overhead crane experimental testbed used for the experiments. Fig. 5b and c show a GBL800E wind blower manufactured by BOSCH that was used to generate the wind as an external disturbance and the wind force was measured using a GM816 digital anemometer. The crane is equipped with a motion mechanism driven by a DC motor and three measuring encoders with a resolution of 4096 pulses per rotation are used for measuring the trolley position, cable length and payload angle. The payload angle can be measured with an accuracy of 0.0015 rad. The real-time implementation involves a Pentium-based personal computer, and a control algorithm designed using the MATLAB/Simulink. The sample time used was set to 0.01 s. Table 2 presents the system parameters of the overhead crane experimental testbed.

Several experiments involving simultaneous hoisting and external disturbances were conducted to verify the real-time performance of the proposed control scheme. Fig. 6 illustrates the input signal $R(t)$ applied for the trolley movement. Due to the limitation of the crane testbed, the payload was hoisted from 0.17 m to 0.59 m (Fig. 7) which involves 71% of the

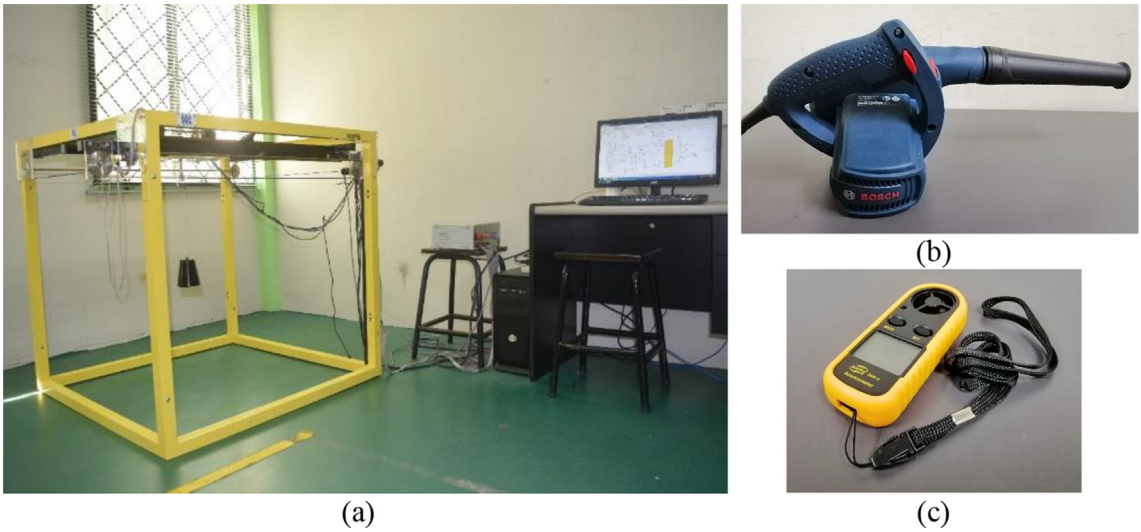

Fig. 5. (a) An overhead crane experimental testbed, (b) GBL 800 E Wind blower, (c) GM 816 Digital anemometer.

Table 2
System Parameters.

System parameters	Values
Hoisting cable length, l	0.17–0.59 m
Gravitational constant, g	9.8ms^{-2}
Viscous damping, b_x	82 Ns/m
Viscous damping, b_l	75 Ns/m
Mass of payloads, m	0.74 kg
Mass of trolley, m_r	1.155 kg

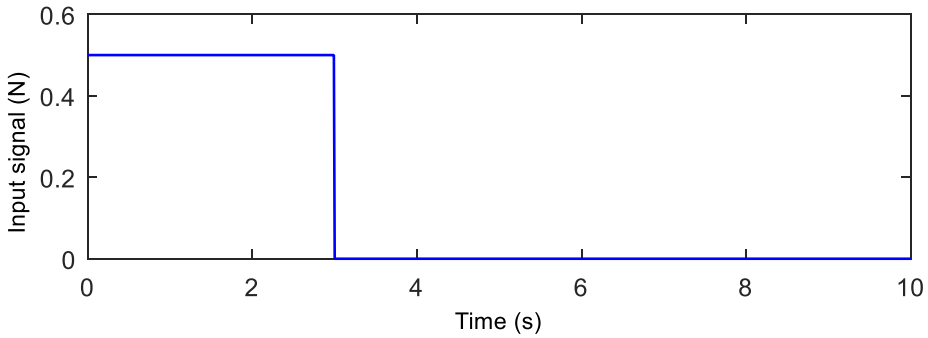

Fig. 6. Input signal of the trolley.

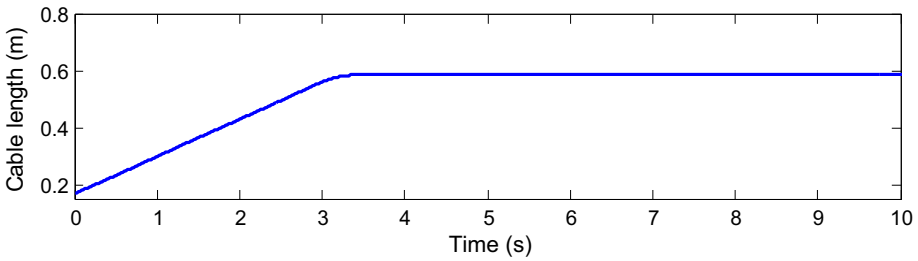

Fig. 7. Cable length hoisting.

height of the crane. During the hoisting, the disturbance was applied by hitting the payload physically, and the disturbance is sustained approximately the same to maintain consistency among different experiments. Furthermore, persistent wind disturbance was implemented with a constant wind speed of 25 ms^{-1}.

To conduct an extensive study, three cases involving the hoisting and disturbance were examined:

- Case 1: The payload was hoisted whilst the disturbance was exerted on the payload mass of 0.74 kg in parallel to the trolley axis during the crane motion.
- Case 2: A non-zero initial condition is considered, with the initial swing angle, $\theta(0) \approx -6^{\circ}$. Practically, this is a case where the trolley and the carried payload initially are not aligned on the same axis.
- Case 3: The payload was hoisted whilst the wind disturbance with a constant speed of 25 ms^{-1} was applied on the payload continuously.

For performance comparisons, a PSO-based PID approach was also combined with the NNUMZV shaper as shown in Fig. 8 and implemented under all the experimental cases. By adopting the same technique in optimizing the APIDLNN initial weights, PSO was utilized to determine the optimal gains for the comparative method through simulation in Matlab. The PSO parameters such as the velocity update of the i^{th} particle and the inertia weight were assigned as in Eqs. (13)–(15),

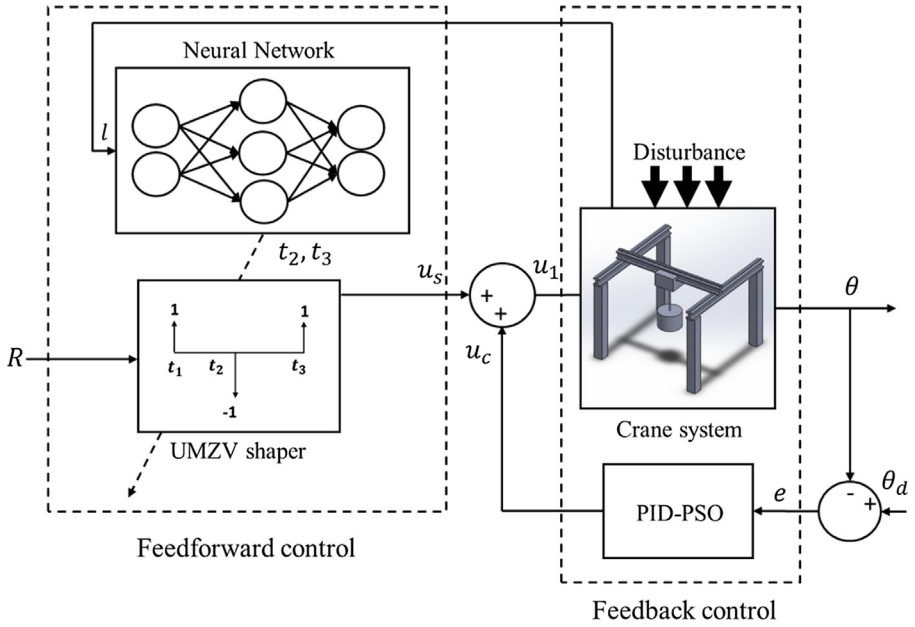

Fig. 8. NNUMZV-PIDPSO control structure.

whereas the optimal PID gains were carefully obtained by minimizing the fitness function as in Eq. (16). The proportional gain K_p, derivative gain K_d and integral gain K_i were deduced as −0.0626, −0.6803 and 0.1387 respectively.

The performances of the controllers were evaluated based on the level of payload swing suppressions and the residual swing (RS) angles when the payload undergoes hoisting and disturbances. As the control aim is to yield a zero payload swing, the mean square error (MSE) can be utilized as a performance index, where an MSE value of a payload swing response gives a total swing angle for a particular period of time. Therefore, a lower MSE value is desirable as it indicates a higher swing suppression. To evaluate the level of swing reductions in a steady state response, the RS was obtained based on the maximum swing amplitude after 6 s of the trolley movements for all cases. A low RS is essential for a fast placement of payload at a desired location.

5.1. Experimental results of the input shaper

The effects of hoisting and disturbance on the payload swing response of the overhead crane experimental testbed were firstly examined for all cases using the NNUMZV shaper proposed in [12]. As the NNUMZV shaper was successfully implemented on the same crane testbed, the network structure in Fig. 3 used the same sets of weights and biases as given in Table 3.

Fig. 9 illustrates the trolley position and the input-shaped signal of the shaper when excited with the input signal in Fig. 6. Fig. 10 shows the payload swing responses for the three cases of external disturbances using the shaper with a payload mass

Table 3
The weights and biases of NNUMZV [12].

The weights between the input and hidden layers w_{ij}						The biases in the hidden layer θ_j		
w_{11}	w_{12}	w_{13}	w_{21}	w_{22}	w_{23}	θ_1	θ_2	θ_3
−7.1048	4.8275	10	−0.1354	−0.1630	10	1.4745	5.7060	−2.2843

The weights between the hidden and output layers w_{jk}						The biases in the output layer θ_k	
w_{11}	w_{12}	w_{21}	w_{22}	w_{31}	w_{32}	θ_1	θ_2
−8.2670	−10	6.4146	10	−5.1801	−9.4777	−3.8218	−9.0687

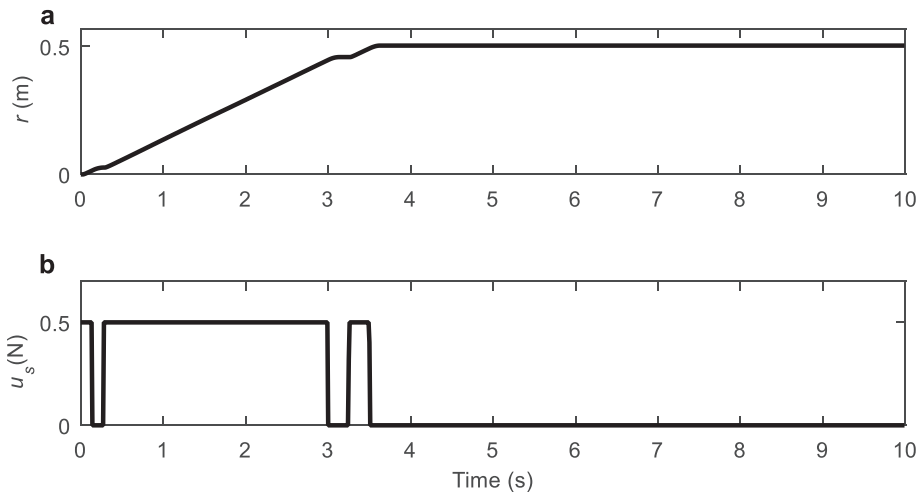

Fig. 9. (a) Trolley position; (b) Input-shaped signal of the shaper.

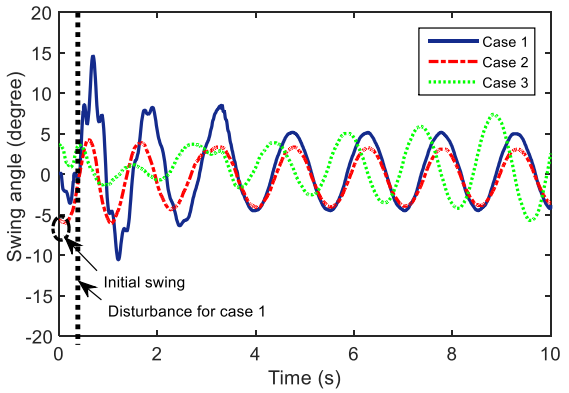

Fig. 10. Payload swing responses of the shaper under payload hoisting and disturbance.

of 0.74 kg. The time instance when the disturbance was applied for Case 1 was shown with vertical dotted lines, which was approximately at 0.4 s. The initial swing angle of $-6°$ is also shown in Fig. 10 for Case 2. Furthermore, the effect of continuous wind force on the payload swing is also illustrated in Fig. 10 for Case 3.

Obviously, high swing responses were observed for all cases with high MSE values as tabulated in Table 4. Table 4 also shows the RS values for all cases, which were high, and thus a longer time is needed for the payload to settle down. The experimental results also imply the unsatisfactory performance of the shaper, due to its sensitivity towards the existence of external disturbances. A swing controller scheme is proposed to enhance the NNUMZV shaper and adapt to the effects of the disturbances.

Table 4
Performance Indices obtained using the NNUMZV shaper.

Experiment	MSE	RS (degree)
Case 1	11.6723	5.1556
Case 2	7.4411	4.6583
Case 3	9.4372	7.3829

5.2. Experiment results of the NNUMZV-APIDLNN algorithm

This section examines performances of the NNUMZV-APIDLNN algorithm to reduce the payload swing subjected to the simultaneous payload hoisting and external disturbances. The experimental results for the trolley position, swing response and control signal using the proposed and comparative methods are shown in Figs. 11–13 for Cases 1–3 respectively.

For all cases, the trolley movement of both methods stopped approximately at 0.4 m within about 4 s. It was noted that, the final trolley positions reached by both methods for each case were found to be slightly different depending on the type of control method used. It is worth mentioning that the desired trolley position can be accurately achieved by adding a feedback control for position tracking.

Noticeably, the proposed method exhibits superior performance in terms of the overall swing reduction and the levels of residual swing when compared with the comparative method for all cases. The proposed controller was shown to be able to handle the effects of the disturbance in Case 1, a nonzero initial swing angle in Case 2 and a wind disturbance in Case 3. These were shown by the changes in the control signals in Figs. 11c, 12c and 13c. Table 5 tabulates the performance indices for the proposed and comparative methods.

Analyzing the overall swing response with the MSE value, improvements of 86%, 45% and 87% were achieved when compared to the NNUMZV-PIDPSO for Cases 1, 2 and 3 respectively. Furthermore, the swing responses by the proposed method settled down faster, in which the RS for all cases were very small. This indicates the proficiency of the proposed scheme as an anti-swing control with improvement at least by 69% over the comparative method.

Almost no residual swing was obtained in all cases resulted from an effective control signal produced by the combined feedforward and feedback control signals. However, the NNUMZV-PIDPSO method was not able to counter the disturbance

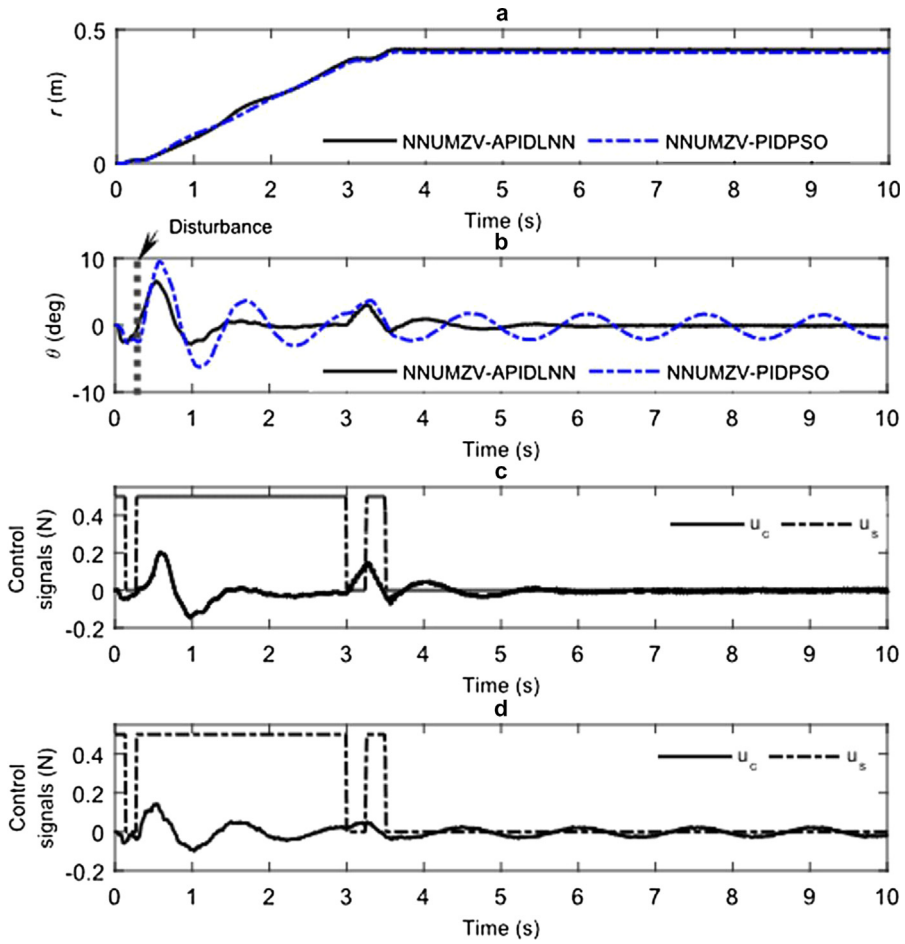

Fig. 11. Experimental results for Case 1. (a) Trolley position; (b) Swing response; (c) Control signals of the proposed method; (d) Control signals of the comparative method.

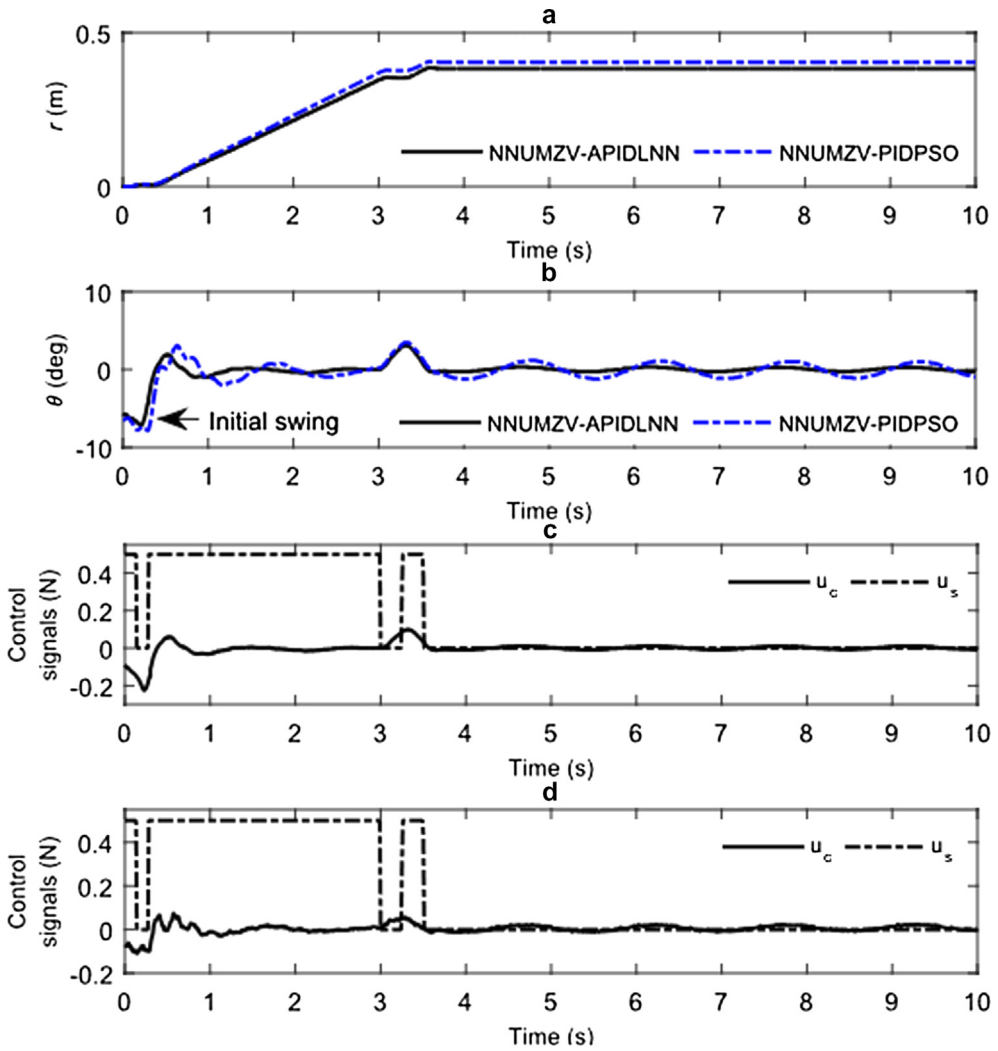

Fig. 12. Experimental results for Case 2. (a) Trolley position; (b) Swing response; (c) Control signals of the proposed method; (d) Control signals of the comparative method.

effect with a large residual swing. For Case 3, although, the trolley moved to a slightly shorter distance, this can be handled by a position controller whereas a higher swing obtained with the NNUMZV-PIDPSO implies that an operator need to wait for a longer time to place a payload at a desired location. The superior performance of the proposed controller is further evidenced in Fig. 14 that show the percentage improvements in the MSE and RS values when compared to the system with the NNUMZV shaper (Table 4).

A successful implementation of the proposed controller relies on the capability of the weights in the APIDLNN to adapt to the external disturbances. A real-time evaluation based on the weight adaptation of the algorithm in real-time was analysed. The variations of weights ($h_{11}, h_{21}, h_{31}, o_{11}, o_{12}$ and o_{13}) are shown in Fig. 15 for the three experimental cases during the trolley motions of 10 s (Fig. 6), which clearly showed the progressive adaptation of the controller to eliminate excessive swing due to the disturbance effects.

For all cases, the rapid change in weight values were varied within 4 s to adapt the effect of the disturbances. For example, in Case 1, when the disturbance was exerted on the payload at approximately 0.4 s (Fig. 11b), there is an immediate change on the weights in Fig. 15 which occur at approximately 0.6 s to reject the effect of the disturbance. The final weight values achieved approximately constant values after 4 s implying that the swing has significantly reduced. These weight adaptations assure that the swing gradually converged towards zero. In addition, the proposed method was capable to adapt and provide a uniform performance under various simultaneous conditions.

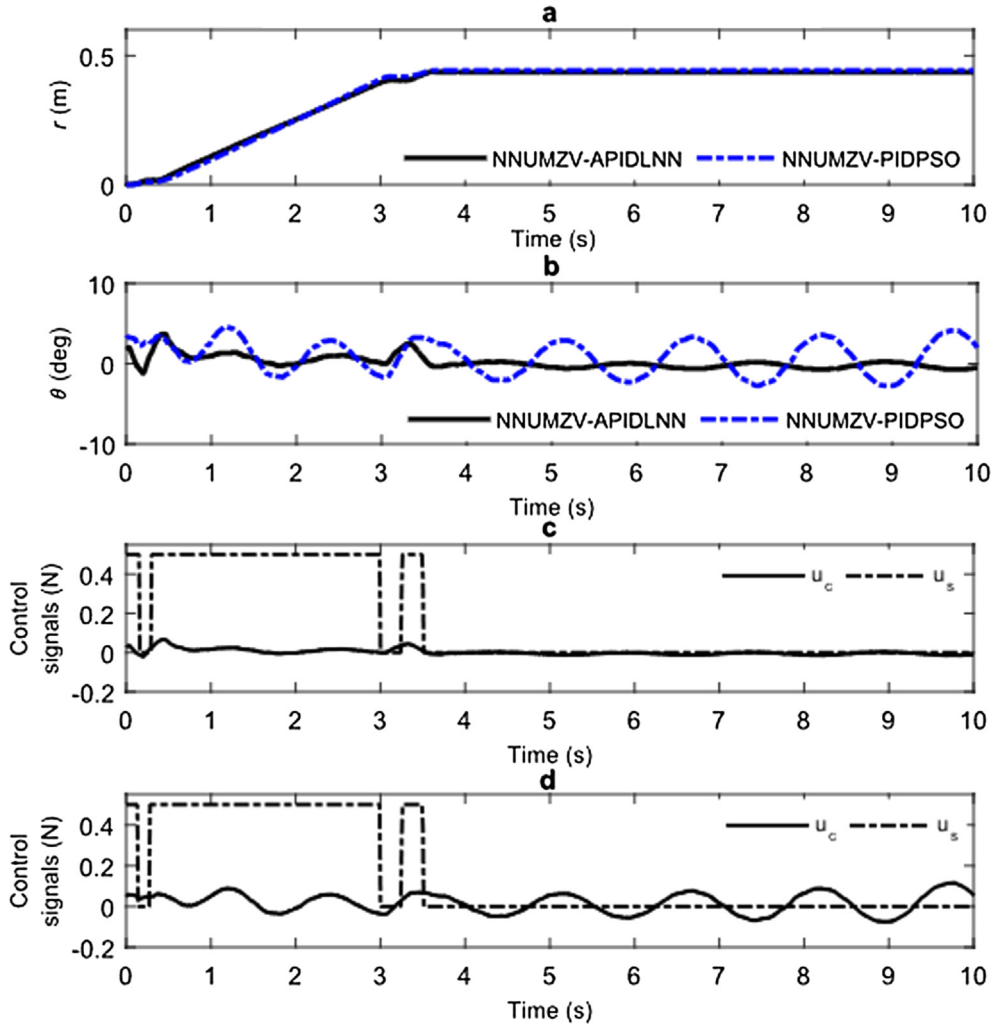

Fig. 13. Experimental results for Case 3. (a) Trolley position; (b) Swing response; (c) Control signals of the proposed method; (d) Control signals of the comparative method.

Table 5
Performance indices for the proposed control method and NNUMZV-PIDPSO.

Cases	MSE		RS (degree)	
	NNUMZV- APIDLNN	NNUMZV- PIDPSO	NNUMZV- APIDLNN	NNUMZV- PIDPSO
Case 1	0.7627	5.6402	0.2301	2.1094
Case 2	1.5880	2.9133	0.3484	1.1063
Case 3	0.6665	5.0763	0.7031	4.1309

6. Conclusion

An efficient control based on an NNUMZV-APIDLNN algorithm was successfully designed and implemented in real-time for swing control of an overhead crane subjected to simultaneous hoisting and external disturbances. The main contribution of this paper is to handle both difficulties simultaneously, which has not been focused in the existing literature. Experimental results with several practical cases showed that the proposed controller attained significant reductions in the overall and residual swings as compared to the NNUMZV-PIDPSO controller. Using the proposed method, the appropriate controller gains can be acquired adaptively in real time, implying that the online learning algorithm with varied learning rates is effective to handle those effects with excellent swing reductions.

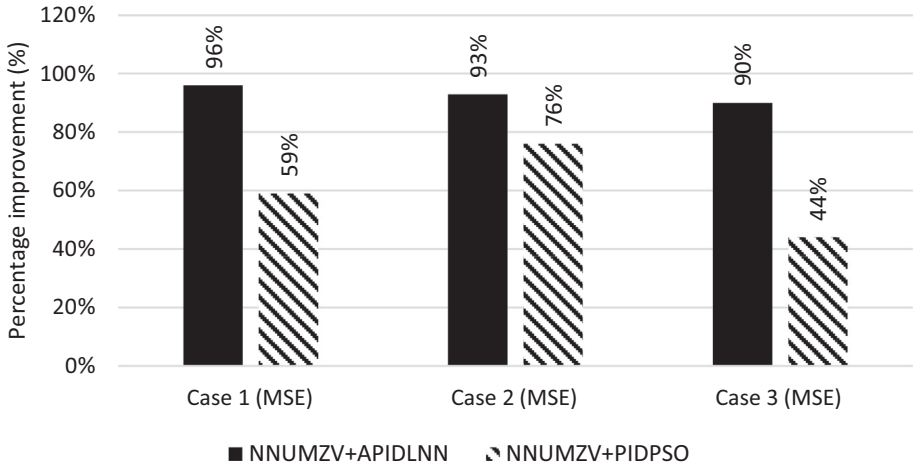

Fig. 14. Improvement in payload swing response as compared to the NNUMZV shaper.

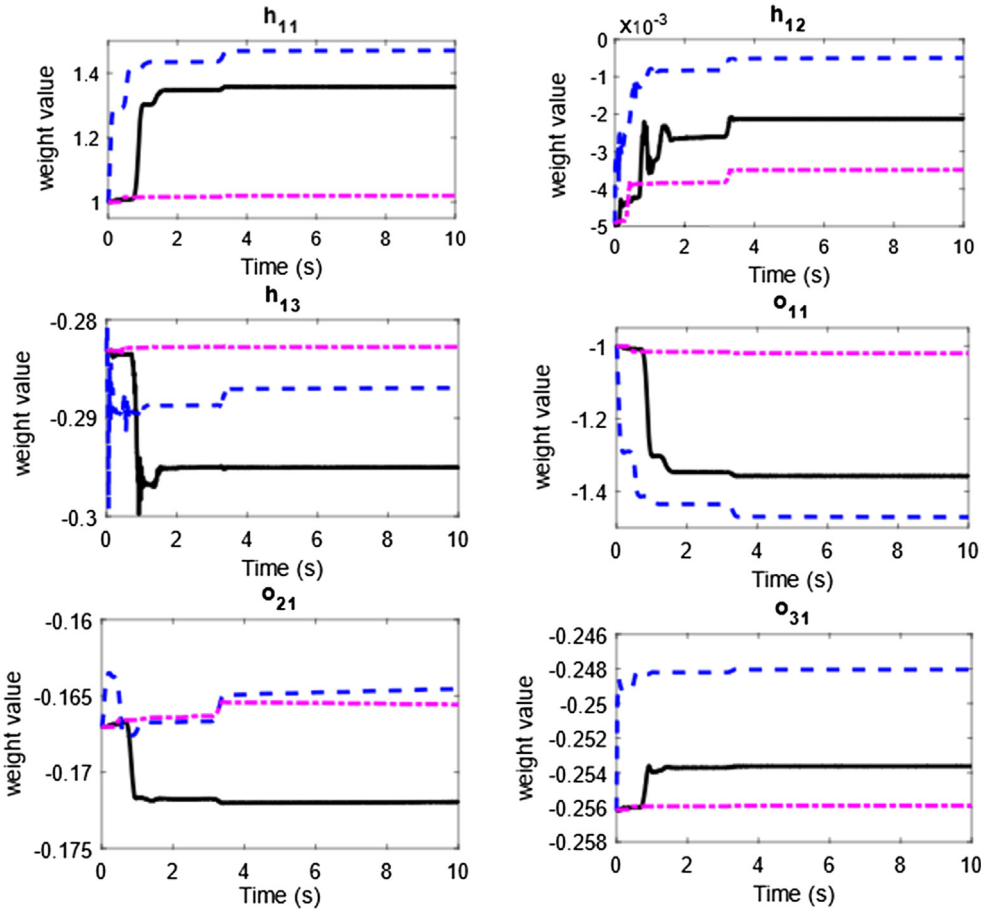

Fig. 15. Weight values of the proposed control method for experimental Case 1 (solid), Case 2 (dashed) and Case 3 (dotted) with external disturbance and non-zero initial swing.

Acknowledgement

The authors gratefully acknowledged the Ministry of Education of Malaysia and Universiti Teknologi Malaysia, Malaysia for the financial support through Fundamental Grant Research Scheme FRGS/1/2018/TK04/UTM/02/38 and Vote No. 5F044.

References

[1] N. Sun, T. Yang, H. Chen, Y. Fang, Dynamic feedback antiswing control of shipboard cranes without velocity measurement: theory and hardware experiments, IEEE Trans. Ind. Inf. 15 (2019) 2879–2891.
[2] N. Sun, T. Yang, Y. Fang, B. Lu, Y. Qian, Nonlinear motion control of underactuated three-dimensional boom cranes with hardware experiments, IEEE Trans. Ind. Inf. 14 (2018) 887–897.
[3] J. Smoczek, J. Szpytko, Particle swarm optimization-based multivariable generalized predictive control for an overhead crane, IEEE/ASME Trans. Mechatron. 22 (2017) 258–268.
[4] H.I. Jaafar, Z. Mohamed, M.A. Shamsudin, N.A. Mohd Subha, L. Ramli, A.M. Abdullahi, Model reference command shaping for vibration control of multimode flexible systems with application to a double-pendulum overhead crane, Mech. Syst. Signal Process. 115 (2019) 677–695.
[5] J. Huang, X. Xie, Z. Liang, Control of bridge cranes with distributed-mass payload dynamics, IEEE/ASME Trans. Mechatron. 20 (2015) 481–486.
[6] X. Zhao, J. Huang, Distributed-mass payload dynamics and control of dual cranes undergoing planar motions, Mech. Syst. Signal Process. 126 (2019) 636–648.
[7] L. Ramli, Z. Mohamed, A.M. Abdullahi, H.I. Jaafar, I.M. Lazim, Control strategies for crane systems: a comprehensive review, Mech. Syst. Signal Process. 95 (2017) 1–23.
[8] J. Vaughan, W. Singhose, Input shapers for reducing overshoot in human-operated flexible systems, , (2009) 178–183.
[9] Y. Zhang, M. Li, J. Zhang, Vibration control for rapid attitude stabilization of spacecraft, IEEE Trans. Aerosp. Electron. Syst. 53 (2017) 1308–1320.
[10] V. Duc, K. Trong, Combination of input shaping and radial spring-damper to reduce tridirectional vibration of crane payload, Mech. Syst. Signal Process. 116 (2019) 310–321.
[11] K.L. Sorensen, K. Hekman, W.E. Singhose, Finite-state input shaping, IEEE Trans. Control Syst. Technol. 18 (2010) 664–672.
[12] L. Ramli, Z. Mohamed, H.I. Jaafar, A neural network-based input shaping for swing suppression of an overhead crane under payload hoisting and mass variations, Mech. Syst. Signal Process. 107 (2018) 484–501.
[13] D. Newman, S.W. Hong, J. Vaughan, The design of input shapers which eliminate nonzero initial conditions, J. Dyn. Syst. Meas. Control. 110 (2018), DS171620.
[14] J. Huang, E. Maleki, W. Singhose, Dynamics and swing control of mobile boom cranes subject to wind disturbances, IET Control Theory Appl. 7 (2013) 1187–1195.
[15] R. Tang, J. Huang, Control of bridge cranes with distributed-mass payloads under windy conditions, Mech. Syst. Signal Process. 72–73 (2016) 409–419.
[16] R. Mar, A. Goyal, V. Nguyen, T. Yang, W. Singhose, Combined input shaping and feedback control for double-pendulum systems, Mech. Syst. Signal Process. 85 (2017) 267–277.
[17] T. Yang, N. Sun, H. Chen, Y. Fang, Neural network-based adaptive antiswing control of an underactuated ship-mounted crane with roll motions and input dead zones, IEEE Trans. Neural Networks Learn. Syst. (2019) 1–14, https://doi.org/10.1109/TNNLS.2019.2910580, In press.
[18] I. Golovin, S. Palis, Robust control for active damping of elastic gantry crane vibrations, Mech. Syst. Signal Process. 121 (2019) 264–278.
[19] H. Zhang, J. Wang, Active steering actuator fault detection for an automatically-steered electric ground vehicle, IEEE Trans. Veh. Technol. 66 (2017) 3685–3702.
[20] H. Zhang, Y. Shi, J. Wang, H. Chen, A new delay-compensation scheme for networked control systems in controller area networks, IEEE Trans. Ind. Electron. 65 (2018) 7239–7247.
[21] Y. Hu, W. Gu, H. Zhang, H. Chen, Adaptive robust triple-step control for compensating cogging torque and model uncertainty in a DC motor, IEEE Trans. Syst. Man. Cybern. (2018) 1–10.
[22] M.I. Solihin, A. Wahyudi, Legowo, Fuzzy-tuned PID anti-swing control of automatic gantry crane, J. Vib. Control 16 (2009) 127–145.
[23] M.J. Maghsoudi, Z. Mohamed, A.R. Husain, M.O. Tokhi, An optimal performance control scheme for a 3D crane, Mech. Syst. Signal Process. 66–67 (2016) 756–768.
[24] D. Qian, S. Tong, S. Lee, Fuzzy-logic-based control of payloads subjected to double-pendulum motion in overhead cranes, Autom. Constr. 65 (2016) 133–143.
[25] L.A. Tuan, Design of sliding mode controller for the 2D motion of an overhead crane with varying cable length, J. Autom. Control Eng. 4 (2016) 181–188.
[26] H. Saeidi, M. Naraghi, A.A. Raie, A neural network self tuner based on input shapers behavior for anti sway system of gantry cranes, J. Vib. Control 19 (2013) 1936–1949.
[27] W. Singhose, L. Porter, M. Kenison, E. Kriikku, Effects of hoisting on the input shaping control of gantry cranes, Control Eng. Pract. 8 (2000) 1159–1165.
[28] K.A. Alhazza, Adjustable maneuvering time wave-form command shaping control with variable hoisting speeds, J. Vib. Control 23 (2017) 1095–1105.
[29] A.M. Abdullahi, Z. Mohamed, M. Zainal Abidin, S. Buyamin, A.A. Bature, Output-based command shaping technique for an effective payload sway control of a 3D crane with hoisting, Trans. Inst. Meas. Control 39 (2017) 1443–1453.
[30] J. Stergiopoulos, A. Tzes, An adaptive input shaping technique for the suppression of payload swing in three-dimensional overhead cranes with hoisting mechanism, in: IEEE Int. Conf. Emerg. Technol. Fact. Autom. ETFA, Patras, Greece, 2007, pp. 565–568.
[31] X. He, W. He, J. Shi, C. Sun, Boundary vibration control of variable length crane systems in two-dimensional space with output constraints, IEEE/ASME Trans. Mechatron. 22 (2017) 1952–1962.
[32] M.J. Maghsoudi, L. Ramli, S. Sudin, Z. Mohamed, A.R. Husain, H. Wahid, Improved unity magnitude input shaping scheme for sway control of an underactuated 3D overhead crane with hoisting, Mech. Syst. Signal Process. 123 (2019) 466–482.
[33] N. Sun, T. Yang, Y. Fang, Y. Wu, H. Chen, Transportation control of double-pendulum cranes with a nonlinear quasi-PID scheme: design and experiments, IEEE Trans. Syst. Man Cybern. Syst. 49 (2018) 1–11.
[34] Q.H. Ngo, K.S. Hong, Sliding-mode antisway control of an offshore container crane, IEEE/ASME Trans. Mechatron. 17 (2012) 201–209.
[35] S. Pezeshki, M.A. Badamchizadeh, A.R. Ghiasi, S. Ghaemi, Control of overhead crane system using adaptive model-free and adaptive fuzzy sliding mode controllers, J. Control. Autom. Electr. Syst. 26 (2014) 1–15.
[36] M. Park, D. Chwa, M. Eom, Adaptive sliding-mode antisway control of uncertain overhead cranes with high-speed hoisting motion, IEEE Trans. Fuzzy Syst. 22 (2014) 1262–1271.
[37] R.M.T. Raja Ismail, N.D. That, Q.P. Ha, Modelling and robust trajectory following for offshore container crane systems, Autom. Constr. 59 (2015) 179–187.
[38] M. Zhang, X. Ma, X. Rong, X. Tian, Y. Li, Error tracking control for underactuated overhead cranes against arbitrary initial payload swing angles, Mech. Syst. Signal Process. 84 (2017) 268–285.
[39] H.H. Lee, Motion planning for three-dimensional overhead cranes with high-speed load hoisting, Int. J. Control 78 (2005) 875–886.
[40] W. Singhose, Command shaping for flexible systems: a review of the first 50 years, Int. J. Precis. Eng. Manuf. 10 (2009) 153–168.
[41] S.S. Gurleyuk, Optimal unity-magnitude input shaper duration analysis, Arch. Appl. Mech. 77 (2007) 63–71.
[42] S. Cong, Y. Liang, PID-like neural network nonlinear adaptive control for uncertain multivariable motion control systems, IEEE Trans. Ind. Electron. 56 (2009) 3872–3879.

[43] F.J. Lin, J.C. Hwang, K.H. Tan, Z.H. Lu, Y.R. Chang, Intelligent control of doubly-fed induction generator systems using PIDNNs, Asian J. Control 14 (2012) 768–783.
[44] Q. Zhang, S. Wang, A. Zhang, J. Zhou, Q. Liu, Improved PI neural network-based tension control for stranded wire helical springs manufacturing, Control Eng. Pract. 67 (2017) 31–42.
[45] R. Wai, C. Liu, Design of dynamic petri recurrent fuzzy neural network and its application to path-tracking control of nonholonomic mobile robot, IEEE Trans. Ind. Electron. 56 (2009) 2667–2683.
[46] J.R. Huey, J. Huey, W. Singhose, Stability analysis of closed-loop input shaping control, IFAC Proc. (2005) 305–310.